FINDING SHORT RANGE ORDER IN HIGH ENTROPY ALLOYS

A Thesis Presented for the
Master of Science
Degree
The University of Tennessee, Knoxville

Mariah Wakefield
May 2024

ACKNOWLEDGEMENTS

I would like to thank Prof. Takeshi Egami for his mentorship and insight. Thank you also to Mr. Wojciech Dmowski for his assistance in analyzing the samples. Last, thank you to Prof. Peter Liaw and Prof. Yanfei Gao for their feedback as part of my master's committee.

ABSTRACT

In this project, chemical short-range order in four samples of the high entropy alloy FeMnAlC was investigated. X-ray diffraction measurements were performed at the Advanced Photon Source of Argonne National Laboratory in Chicago, IL. The data were then analyzed by curve fitting with mathematical Gaussian and Lorentzian functions. Conditional fitting was applied to the first and fourth samples to confirm the original curve fit. Conditional fitting was then used to adjust the determined indices of the Gaussian peaks in these samples so that they better reflected what was occurring in nature. From these indices, an increased unit cell was predicted with four atoms, further confirming chemical ordering. The peak width of the Gaussian and Lorentzian peaks in each of the four samples was found by determining the full width at half maximum (FWHM). Using the FWHM, the number of unit cells in short-range ordering was calculated for each of the peaks. The peak height was also examined to determine the strength of short-range ordering. The strength of short-range ordering for each of the peaks in the four samples was then ranked from highest to lowest. Finding short-range order can give information that helps explain the mechanical properties of high entropy alloys. Because of their exceptional properties, applications of high entropy alloys include various fields such as aerospace.

TABLE OF CONTENTS

LIST OF TABLES

LIST OF FIGURES

LIST OF EQUATIONS

CHAPTER ONE: INTRODUCTION AND GENERAL INFORMATION

What are high entropy alloys (HEAs)? A central consideration is that of entropy. The configurational entropy of mixing per mole is expressed by delta Smix in Equation 1 below. In this equation, R is the gas constant, c_i is the molar fraction of the i-th element, and n is the total number of elements. Furthermore, consider Figure 1 below. As shown in the contour plot (this case being for a ternary alloy), the closer the alloy composition to the central region, the larger the delta Smix value. An energy gain occurs, and this energy gain is sufficient for the entropy level to stabilize the random solid solution phase against intermetallic compounds. The random solid solution is stabilized, hence the 'high-entropy effect', when the elements are in an equimolar fraction. Now, consider Figure 2 below. Elements are randomly mixed, represented by circles of different colors, into a multicomponent alloy. In the figure, equal atom size and loose atomic packing are assumed. The configurational entropy of mixing is maximized because of the equiatomic composition of the alloy [1].

$$\Delta S_{mix} = -R \sum_{i=1}^{n} c_i \ln c_i$$

Equation 1. Configurational Entropy of Mixing [1]

Under certain conditions, patterns emerge in the multicomponent alloy. These patterns are of interest to this project. For context, some definitions are needed. First, long-range order describes atomic arrangement below the critical temperature. When a solid solution is cooled below a certain critical temperature, the atoms arrange themselves and become ordered.

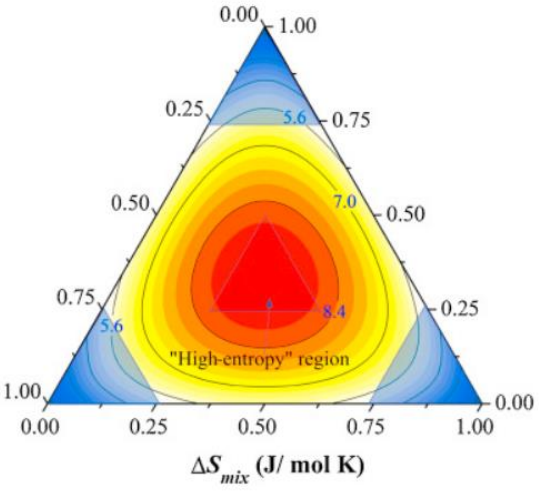

Figure 1. The contour plot of an example ternary alloy [1]

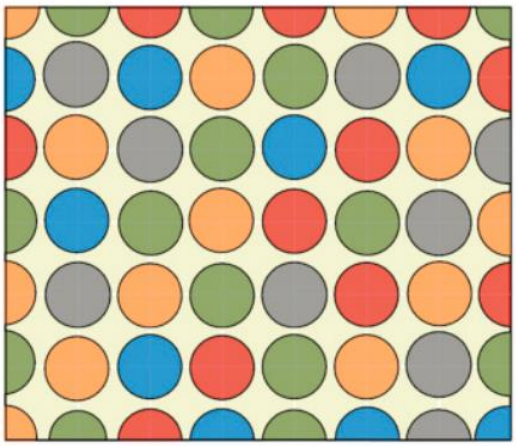

Figure 2. Random mixing of elements in a multicomponent alloy [1]

This periodic arrangement persists along long distances in the crystal. Above the critical temperature, the atomic arrangement loses long-range order and becomes more random, but retaining some local order, short-range order (SRO). Under these conditions, two options are available. Short-range order is when long-range order disappears and the atomic distribution becomes more or less random. Perfect randomness is not achieved, and the tendency is for unlike atoms to be nearest neighbors. However, clustering is when like atoms have a tendency to be nearest neighbors.

Scientists are still searching for methods to describe short range order. For example, short-range order can be represented by Warren-Cowley parameters. Warren-Cowley parameters describe order in a specific coordinated arrangement. The observed concentration of an atom type is compared to that predicted by stoichiometry. An example is shown in Equation 2 below. The first numerator describes the probability of finding a B atom at a position from an origin placed on an A atom. The second numerator is vice versa. c_A and c_B are defined as the atomic fractions of A and B atoms in the alloy [5].

$$\alpha_{lmn}^{AB} = 1 - \frac{P_{lmn}^{AB}}{c_B} = 1 - \frac{P_{lmn}^{BA}}{c_A}$$

Equation 2. Definition of Warren-Cowley parameter [5]

Finding short-range order is of emerging significance within high entropy alloy research. A salient example is that short-range order can give information concerning the mechanical properties of high entropy alloys. Consider turbine blades used in jet engines. Prof. Egami explained that with long range order, the jet engine blade could become brittle. Short-range order provides a unique solution. The engine blade exhibits improved strength but is not brittle.

Indeed, when considered for such applications, high entropy alloys exhibit improved fatigue behavior and lifetime projections. Cyclic stress is an important element in aviation engines. Hemphill studied the fatigue behavior to the high entropy alloy $Al_{0.5}CoCrCuFeNi$. The results were compared with that for many conventional alloys such as steels and titanium alloys. The fatigue characteristics compare favorably to that of the conventional alloys. Figure 3 below shows the typical stress range vs. the number of cycles to failure curve. The lower limit of the fatigue ratio for the HEA is higher than that of different steels, titanium, and even zirconium alloys. Certain materials, such as ultra-high strength steels and wrought aluminum alloys, have lower fatigue ratios in spite of higher tensile strength because of their brittle nature. HEAs such as the one in consideration exhibit high fatigue ratios in comparison with materials of equal tensile strengths. HEAs such as the example have reduced fault densities. High entropy alloys can be combined with other alloys such as superalloys for aerospace applications. The different operational temperatures, pressures and stress levels force the use of a combination of materials. Due to its increased stability over a larger temperature range and over a longer time period, high entropy alloys are still effective at higher temperatures. Aerospace engines need materials that can withstand high rotational speeds, creep, fatigue fractures, and high temperatures [2].

The aim of this research was to detect and glean information from the short-range order present in the sample. X-ray diffraction measurements were performed at the Advanced Photon Source (APS) of Argonne National Laboratory. As will be discussed further, the experimental data were analyzed using curve fitting software in MATLAB R2023a. A curve of best fit was found using a range of Q values. Conditional fitting was then applied and compared to the original curve fit. The purpose was to check conditional fitting, check the error related to Q values, check the indexes of the gaussian peaks, determine if short range order is present, and

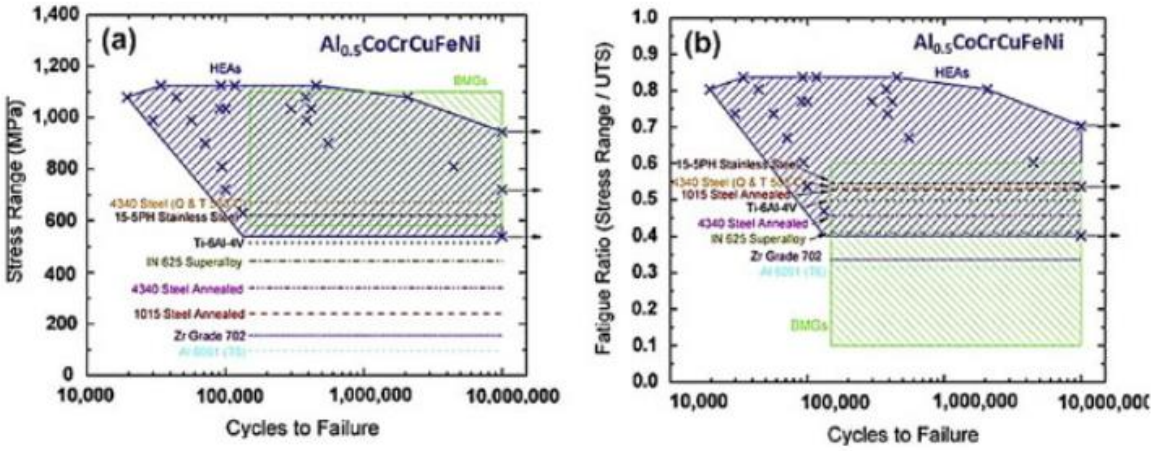

Figure 3. (a) Comparison of Stress Range vs. Cycles to Failure (b) Comparison of Fatigue Ratio vs. Cycles to Failure [2]

determine what type of short-range order. Analysis of the experimental data using the curve fitting software could reveal important information about the physical characteristics of the samples.

The following sections of this thesis paper are described below. Literature Review discusses existing research on short-range ordering. Materials and Methods describes the experimental processes used to obtain data and generate results. Results and Discussion displays plots of the x-ray diffraction data, relevant calculations, as well as interpretation and analysis of the results. Conclusions and Recommendations discusses conclusions reached from data analysis, with important findings and reflections.

CHAPTER TWO: LITERATURE REVIEW

Research is currently being performed to examine the formation of short-range order (SRO) in high entropy alloys as well as the effect on mechanical properties. This first paper uses the context of binary alloys to introduce clustering and short-range order in high entropy alloys. For instance, the difference between clustering and short-range order seemed blurred in multicomponent alloys due to the presence of various localized substructures, nanosized domains or superlattices, ordered interstitial complexes, and topological ordering. For medium entropy alloys and high entropy alloys, the concept of short-range order was extended to refer to either chemical or topological deviation from randomness in the interatomic scale. However, the deviation is still not enough to form nanoscale precipitates.

Scientists reported short-range order in different types of high entropy alloys. For instance, SRO was found in the FCC alloy FeCoNiCrCuAl, in which Al has a larger atomic size than the other elements. Also, the deviation from average of the local atomic environment was observed in the first and second atomic shell for Zr- and Hf- containing BCC refractory HEAs. SRO has been discovered even when there is small atomic size difference. An $L1_2$-type $(Fe, Co, Ni)_3Cr$ ordering was found in the FCC alloy FeCoCrNi; there was not a great difference in atomic size. The formation of SRO in this HEA was apparently caused by different spin directions between Cr and the other elements and the differing electronic structures between the elements. SRO has been found to exist in the BCC refractory alloy NbMoTaW, which has relatively small atomic size differences, due to the different bonding energies of the elements. SRO seems to have a high tendency to form in HEAs and is tied to their chemical complexity. As the number of elements increases, the formation of SRO seems to be harder due to the intricate atomic environment. Considering thermodynamics, the formation of SRO in HEAs

could be due to fluctuation in the local strain, bonding states, or electronic and magnetic interactions.

As previously stated, short-range order can have an effect on the mechanical properties of high entropy alloys. SRO can affect the dislocation glide resistance or the classical Peierls-Nabarro resistance. Existence of SRO can also change the stacking fault energy. For instance, SRO can make the Suzuki mechanism no longer valid for describing solute atoms within stacking faults. Considering deformation, SRO can affect dislocation motion, twinning, and phase transformations. SRO represents the fluctuation of the local atomic environment and the effect on deformation may vary in different types of HEAs. The effect on the Peierls-Nabarro resistance and the stacking fault energy allows for large fluctuated lattice resistance, complex dislocation maneuvers, and other behaviors in FCC HEAs. The effect of deformation and SRO varies from site to site. In BCC high entropy alloys, SRO primarily affects the dislocation behavior, such as increasing dislocation core energy, pinning dislocations, and promoting cross-slip and multiplication [3].

Another paper discusses the role of short-range order in strengthening high entropy alloys. Short-range order strengthening or short-range order hardening is known as one of the principal strengthening mechanisms in solid solution. However, it is not accepted by everyone. One author cites short range order only as associated with Cu-Au alloys in spite of describing solid solution strengthening in detail, including the effect of solute drag to dislocations. Flinn was probably the first to apply a thermodynamic model to quantitatively predict the effect of short-range order hardening. Flinn applied Cowley's nearest neighbor model to calculate the APB energy. The author applied the model to Ag-Au alloys reaching a maximum value of 2.5 MPa at 50 at% Ag, which is a three-fold increase compared to the mechanical mixture value.

Another author, Mohri, applied the cluster variation method, which includes interactions between nearest and next nearest neighbors, to calculate APB energies and to estimate the hardening effect in FCC alloys. Prototype calculations were performed in which the interactions were varied to obtain different SRO parameters. The results show a three- to five- fold increase in strengthening effect. This example and others like it connect SRO hardening to an increase in yield strength. SRO strengthening is also described as a "friction hardening" effect and causes a dragging force that acts on dislocations in its movement.

Another salient example of SRO hardening involved the ultimate tensile strength of Fe-Al alloys. The tensile strength is affected in the same way as yield strength as the aluminum concentration increases. The hardening is a friction stress effect, and Portevin-Le Chatelier and discontinuous yielding is observed. These observations are expected in high temperature deformation, since diffusional relaxation matches the time scale of gliding. As another example, refractory high entropy alloys are characterized by high short range order parameters. SRO hardening has been shown to play in important role in determining the strength of high entropy alloys. This mechanism acts in the whole strain path (and not only in yielding), which explains why ductility is not compromised. SRO hardening has no relation to the maximum configurational entropy, which means that the effect is valid for all concentrated compositions and not only for the equimolar composition [4].

Finally, a different paper discusses determining short-range order using total scattering techniques. Short-range order can explain physical phenomena such as strengthening, thermodynamic discontinuities, and electrical resistivity. However, conventional analysis using x-ray diffraction only provides information about the long-range order of the sample. With total scattering both the Bragg and diffuse scattering are considered [5]. This is especially relevant to

my research. In my research, the diffuse scattering region is considered in detecting and determining the types of short-range order present. As will be discussed further in my thesis, information can be gleaned from the Bragg peaks as well as any diffuse or weak peaks. Diffuse or weak peaks are especially important in determining short range order. Returning to this paper, total scattering is used to determine if short-range order is present in the sample Cu_3Au.

When considering ordering transitions in solid solution, the Cu-Au alloy system is often used. Below a certain critical temperature, two long-range ordered cubic structures are formed. Cu_3Au is a prominent example when studying these transitions. A single crystal x-ray diffraction study was carried out using Cu_3Au. Close to T_c, diffuse scattering was observed, which apparently indicated the presence of the $D0_{22}$ and $L1_2$ structures. As the temperature increased, the observed $D0_{22}$ pattern disappeared while a diffuse maximum was observed. Computer simulations based on the diffuse data gathered suggested specific heat anomalies at 600 degrees Celsius due to $D0_{22}$ micro-domains and at 850 degrees Celsius due to $L1_2$ structures. These studies suggest that an ordering transition is preceded by a region in which short-range order is observed. The experiment in this paper uses in situ x-ray total scattering to determine the short-range order in Cu_3Au. The RMC method is used to provide understanding about ordering beyond just using Warren Cowley parameters.

In this experiment, x-ray diffraction patterns were collected. The position of the Bragg peaks is slightly shifted with temperature, and is associated with the change in lattice parameter due to thermal expansion. There is also an increase in the Debye-Waller factor. Three of the data sets show evidence of $L1_2$ super lattice peaks. Careful inspection showed an increase in the diffuse scattering signal as the temperature was reduced towards the ordering temperature. Fitting the data using a Rietveld refinement, the phase fraction is negligible and does not have a

measurable contribution to the PDF. There is a reduction in lattice parameter with temperature. This reduction is expected, as the $L1_2$ structure that forms the Au atoms is surrounded by Cu atoms. The lattice is allowed to contract due to the removal of Au-Au correlations.

RMC fitting was carried out using supercells that came from the unit cells from Rietveld refinement. The data was corrected for the instrumental resolution and calculated from a consideration of the full width at half maximum. RMC refinements were carried out using boxes that contained a random distribution of atoms. Any remaining discrepancies must be due to changes in site occupancy or chemical ordering. Neutron data was collected from a room temperature as-sprayed Cu_3Au powder. For x-rays, the scattering strength is proportional to the atomic number. There is a large scattering contrast between Cu and Au atoms. For neutrons, the scattering lengths are very close. As such, chemical ordering in a Cu-Au alloy would be invisible in neutron data. Neutron scattering can confirm ordering observed in x-ray data, and whether it is not just a consequence of RMC fitting.

The data presented for the Cu_3Au system demonstrates the ability to analyze subtle variations of order in metallic systems using a combination of PDF and RMC techniques. Comparing the ordering observed experimentally with predictions from a random model allows for insights into the ordering without using one dataset as a systematic baseline. Avoiding errors in data processing is important in successfully determining the order present. Cu_3Au was observed to undergo an ordering transition at 400 degrees Celsius, which agrees with literature values. This transition was shown by the appearance of superlattice Bragg peaks and a change in the area under the peaks in the PDF. Prior to the transition, different levels of short-range order were present, as depicted by changes in the PDF [5].

CHAPTER THREE: MATERIALS AND METHODS

The research described is both qualitative and quantitative. The research is qualitative for a couple of reasons. First, a conceptual understanding is needed of short-range ordering in high entropy alloys as well as the methods below. Also, involved is the visual inspection and comparison of graphs. The research is also quantitative. X-ray diffraction measurements were made with focus on the diffuse scattering region. The gathered data was visually represented using computer software and quantitative methods were used to analyze the data. Details of the experimental aspects are discussed below.

X-ray diffraction data was measured for four samples of the high entropy alloy FeMnAlC: femn-1-1-01792 (Sample 1), femn-1-2-01794 (Sample 2), femn-1-3-01796 (Sample 3), and femn-1-4-01798 (Sample 4). The sample composition was 1:1:1:1. However, the samples were processed differently by annealing at different temperatures. Sample 1 was annealed at 1000 degrees Celsius for 90 seconds. Sample 2 was annealed at 1000 degrees Celsius for 90 seconds, then 550 degrees Celsius for 10 minutes. Sample 3 was annealed at 1000 degrees Celsius for 90 seconds, then 500 degrees Celsius for 30 minutes. Sample 4 was annealed at 1000 degrees Celsius for 90 seconds, then 550 degrees Celsius for 3 minutes. Preparing the samples required arc melting in a copper mold. The samples were then cut and polished. Sample size was 1.5 mm thick by 4 x 6 lateral dimension. A former MIT faculty member now at the University of Wisconsin was involved in preparing the sample.

The measurements were taken by members of the research group under Prof. Takeshi Egami. The experiment was performed at beamline I-D-BC at the Advanced Photon Source (APS) at Argonne National Laboratory in Chicago, IL in the summer of 2022. The incident x-ray energy was 100 keV. A two-dimensional Perkin-Elmer detector was used, with 2850 x 2850

pixels placed 40 cm behind the sample. Each pixel size was 150 micron x 150 micron. Our group used CeO_2 for calibration and a Fit2D software for data processing. Thankfully, I acknowledge that I was present and involved in the gathering of data. The experimental data was analyzed using MATLAB R2023a. Ancillary software products for representation include Microsoft Excel, OriginPro, and SigmaPlot. Calculations were made to adjust the data, and the adjusted data was displayed using Microsoft Notes. Curve fitting software in MATLAB was used to fit plots generated from the experimental data. Then, conditional fitting approaches were used. MATLAB was also used in error analysis.

Initially, Microsoft Excel was used to plot the data collected, but Excel was not the first choice of computer software. Excel was not always easy to use, and curve fitting analysis could not be performed. From my experiences with chemical engineering, I was more familiar with Matlab. The curve fitting software was effective, as I was able to apply custom equations in my curve fit. The error involved in curve fitting was reasonable, and I was able to achieve a decent fit four each of the four samples. The other software programs mentioned were available and used as a backup to MATLAB.

CHAPTER FOUR: RESULTS AND DISCUSSION

For the experiment, x-ray diffraction measurements were taken for each of the four samples. In determining short-range order, a seemingly flat region of the data was focused on over a range of Q values. This region is called the diffuse region. After zooming in to take a snapshot, broad peaks are seen and also some other naturally occurring weak peaks. These broad peaks contain a wealth of information. In this discussion, peak width should be considered. With long-range order, the peak becomes sharp, as seen in the Bragg peaks. Peak width varies inversely to the range of order. A thin peak suggests long-range order, while a broad peak suggests short-range order. This is related to the fact that short-range order may disappear when heat-treated at very high temperatures, while long-range order keeps going.

After plotting the diffuse region, a curve fit was applied using Gaussian and possibly Lorentzian peaks. Curve fitting was applied for several reasons. Using a curve fit allows for better visual representation of the data. In order to obtain a better curve fit, noisy regions of the data were eliminated. In curve fitting, we wanted to apply a custom equation that best represented the data. From this equation, we can glean helpful information from the coefficients. Information from curve fitting can give insights into the chemical ordering in the samples.

After curve fitting, evaluating the goodness of fit can give information about the extent of error. The sum of squares due to error is large for each of the four samples, but this may be due to having a larger data set. A positive note is that both the R-Square and Adj R-Square are close to 1. Having R-Square close to 1 means that a greater proportion of variance is accounted for by the data fitting. In addition, having Adj R-Square close to 1 indicates a better fit. A lower Root Mean Squared Error gives a better prediction of fit. As such, the first sample seems to exhibit the least deviation from the curve fit to the data.

To calculate the integrated intensity, the area under the curve was found for a range of Q values for each of the four samples. The area can give information about short-range order. If there is no short-range order, the integrated intensity would be zero. The greater the integrated intensity, the greater the short-range order. However, the integrated intensity in the diffuse region must be normalized by the integrated intensity of the (111) peak of each sample. Then, the extent of short-range order can be compared. After normalization, the four samples have a similar degree of short-range order. The femn-1-1-01792 sample has a slightly lower amount of short-range order than the other samples, with a value of 0.2938. The femn-1-2-01794 sample narrowly has the highest amount of short-range order at 0.3236. These small differences may not be large enough to show a distinction between the samples.

After normalization to get a sense of the degree of short-range order, the next step was to index the Gaussian peaks that made up the overall peaks in the diffuse scattering region. Using the (111) peak for each of the samples, the lattice constant for each sample was calculated. Then, ratios were taken of the positions of the Gaussian and Lorentzian peaks and a few Bragg peaks to glean information. Using the ratio of the Gaussian or Lorentzian peak to the (111) peak, the peaks were able to be indexed. A conditional fitting process was then applied to see if a better curve fit could be obtained. The indices were used to calculate Q values, which were specifically input into the curve fitting software.

However, the initial curve fits for each of the four samples of the diffuse scattering region were very hard to improve upon. This was seen in the application of conditional fitting using the indices of the peaks. The new conditional curve fits for each of the four samples had great room for improvement. The second and third samples were better than the first and fourth samples.

After careful analysis, comparison of Q values showed some discrepancy. For instance, for Sample 2, the first Gaussian peak had a calculated value of Q = 0.609 inverse Angstroms. The original Q value was 1.14 inverse Angstroms. This shows that there might be a problem with indexing, as the calculated value of Q and the original should be within ten percent of each other. The index was (0.5, 0.5, 0). This index might need to be changed.

For Sample 2, the values for the second gaussian peak and the Lorentzian peak were close. The second gaussian peak had a calculated Q value of 1.361 inverse Angstroms as compared to an original Q value of 1.51 inverse Angstroms. The Lorentzian peak had a calculated Q value of 1.721 inverse Angstroms as compared to an original Q value of 1.7 inverse Angstroms.

There has been discussion about possible improvement in the curve fits, but I did not think much improvement was possible. However, working with Sample 1, the curve fit from conditional fitting has shown drastic improvement after adjusting Q values. In MATLAB, b1 and b2 can represent fixed Q values. The new Q value for the first Gaussian peak in Sample 1 was 0.8010 inverse Angstroms. The new Q value for the second Gaussian peak in Sample 1 was 1.5 inverse Angstroms.

After adjusting Q values, a drastic improvement was shown in the curve fit from conditional fitting for Sample 4. As before, in MATLAB, b1 and b2 can represent fixed Q values. The new Q value for the first Gaussian peak in Sample 4 was 0.9 inverse Angstroms. The new Q value for the second Gaussian peak in Sample 4 was 1.55 inverse Angstroms.

In the first attempt at conditional fitting, the Q values were calculated based upon a guess at the indices of the peaks. From those initial Q values, additional guesses of Q values were made in the conditional fitting process. As previously discussed, ideally the Q value from

conditional fitting should fall within ten percent of the original. For Sample 1, the greatest discrepancy in Q values seems to come from the first Gaussian peak. The percent error is still high, but the latest conditional fitting attempt is much better than the first attempt. This suggests that the index for the first Gaussian peak of Sample 1 needs to be changed. The new Q value obtained from the latest conditional fitting attempt could be used to determine a better index for the first peak.

For Sample 4, similarly the greatest discrepancy in Q values seems to come from the first Gaussian peak. This suggests that the index for the first Gaussian peak of Sample 4 needs to be changed. The current index again is (0.5, 0.5, 0). The new Q value obtained from the latest conditional fitting attempt could be used to determine a better index for the first peak.

As previously identified, the index for the first Gaussian peak of Sample 1 needed to be adjusted. Using Q = 0.8010 inverse Angstroms, an index of (0.25, 0.75, 0) was calculated. The index proved to be a much better representation of the first Gaussian peak. Applied in conditional fitting, the index was used to calculate a new Q value of 1.345 inverse Angstroms. However, the Q value for the second Gaussian peak could improve as well. Using trial and error, a new Q value of 1.6 inverse Angstroms was used to improve the curve fit as shown above. This new Q value is an improved guess and is still within 10 % of the original. As such, the index of (1, 0, 0) for the second Gaussian peak of Sample 1 is still a good estimate.

Again, for Sample 4, the index for the first Gaussian peak needed to be changed. Using Q = 0.9000 inverse Angstroms, an index of (0.25, 0.75, 0) was calculated. Applied in conditional fitting, the index was used to calculate a new Q value of 1.3606 inverse Angstroms. The Q value for the second Gaussian peak could also improve. Using trial and error, a new Q value of 1.65 inverse Angstroms was used to improve the curve fit as shown above. The latest conditional

fitting attempt shows drastic improvement in error percentages, especially the first Gaussian peak. Qualitatively, the conditional fit seems to be an improvement over the original curve fit. An index of (1, 0, 0) is still a good estimate of the second Gaussian peak.

Still another step was to consider the updated indices for the first and fourth samples. These indices were given by nature. Physical interpretation of the results is needed. For the first Gaussian peak of the first and fourth samples, the index was adjusted from (0.5, 0.5, 0) to (0.25, 0.75, 0). Consider a unit cell with lattice constant a. Under normal conditions, a would be 1. For an index of 0.5, the lattice constant would have to double. Therefore, for an index of 0.25, the lattice constant would increase by a factor of four, which means that the unit cell has expanded by a factor of four. So, for the samples, an increased unit cell is seen.

What would cause a unit cell to increase? While there are forces acting on the atoms, lattice distortion would not cause a unit cell to increase. Atomic size or electronegativity mismatches would also not be much of a factor. However, ordering causes the lattice constant to increase or the unit cell to increase. Consider for example, the alloy CuAu. Disorder causes only one atom to be in the unit cell, while ordering causes two atoms to be in the unit cell. The improved index suggests that the unit cell has four atoms, A-B-C-D. These four atoms could possibly be the four elements Fe, Mn, Al, and C. Atomic forces prefer ordering. The increased lattice constant or unit cell suggests that short range order is present.

As another consideration, peak width and peak height can give the range and strength of short-range order in the samples. Looking at the peak width of the Gaussian peaks can give information about how short or how long is the order. From the graph, the information is given in Q space. As previously noted, a custom equation in MATLAB was used in curve fitting. One of the parameters, the c values, give sigma Q. This value can be converted to sigma R in real space,

which can then be used to calculate the full width at half maximum (FWHM) for each of the Gaussian peaks. This was done for the Gaussian peaks in the first and fourth samples. The lattice parameter for each of the four samples was already determined using the (111) Bragg peak in each of the samples. Dividing the FWHM by the lattice parameter, the number of unit cells represented by each Gaussian peak can be calculated. For example, the first Gaussian peak in the first sample represents ordering with a range of 0.850 unit cells. The second peak has ordering with a range of 2.561 unit cells. In each sample, the two Gaussian peaks represent two different types of ordering. This fact is also seen in that the indexes for the two Gaussian peaks are different. For example, the first Gaussian peak in the first sample has an index of (0.25, 0.75, 0). The second Gaussian peak in the first sample has an index of (1, 0, 0). These two different types of order are coexisting in the sample. However, x-ray diffraction is unable to identify the location of the different types of short-range order. In addition, peak height or the intensity can give information about the strength of short-range ordering. The values in the graphs above are given in Q space, but are proportional to the values in real space. In the first sample, short-range ordering represented by the first Gaussian peak is much stronger than that represented by the second Gaussian peak. In the fourth sample, the strength of short-range ordering is similar between the two Gaussian peaks.

After further review, the second and third samples were also considered. The peak width and peak height were found for each of the Gaussian and Lorentzian peaks using the process as noted above. A particular area of interest was the strength of short-range ordering, which has been discussed in terms of peak height. However, a step further can be taken to give a better sense of the strength. Strength of ordering describes which peak is more ordered and is also related to temperature. As shown above, the peak height is in Q space. The product of the peak

height and sigma Q was calculated for the Gaussian and Lorentzian peaks in each of the four samples. Then, this updated value for the strength of ordering in each peak was compared, and the peaks were ranked from highest to lowest. The first Gaussian peak in the first sample shows the strongest amount of ordering, followed by the first Gaussian peak in the fourth sample. The first Gaussian peak in the second sample shows the lowest amount of short-range ordering.

FOR FIGURES/TABLES IN RESULTS, PLEASE REFER TO THE APPENDIX

CHAPTER FIVE: CONCLUSIONS AND RECOMMENDATIONS

From both a qualitative and quantitative standpoint, short-range order was determined to be present in the four samples. This was first seen by examining a certain region of the x-ray diffraction data. Upon zooming in over a certain Q value range, broad and other weak peaks were discovered that give important information. From calculating the integrated intensity, each of the four samples have a similar degree of short-range order. Using MATLAB R2023a, curve fitting software was used to find a best fit of the experimental data. The best fit was found using mathematical Gaussian and Lorentzian functions. Then, conditional fitting was used and suggested that the original indices needed to be adjusted to better represent what was occurring in nature. The updated indices suggested a lattice constant that increased by a factor of four. A unit cell increased by a factor of four with four elements was suggested. Atomic ordering can cause the lattice constant to increase or the unit cell to increase. Thus, the increased lattice constant and unit cell confirm short-range order.

Further information can be given from examining peak width and peak height. The peak width of each the two Gaussian peaks confirm the range of short-range order represented by the peaks. For example, the range of short-range order represented by the first Gaussian peak of the fourth sample is 1.009 unit cells. The two Gaussian peaks represent two different types of short-range ordering that are coexisting in each sample. However, x-ray diffraction does not reveal the locations of short-range ordering in the samples. Peak height gives information about the strength of short-range ordering. A step further was taken to calculate the product of the peak height and sigma Q. This value was used to rank each of the peaks in terms of strength of ordering. In this process, the Gaussian and Lorentzian peaks of the second and third samples were also considered. Although analysis suggests the presence of four atoms in the unit cell, the

types of short-range order described by specific atomic correlations is beyond the scope of this experiment. Further investigation into the interatomic relationships and the locations of chemical ordering is recommended. Another recommendation is to consider the other smaller weak peaks, some of which were counted as noise when examining the diffuse scattering region.

LIST OF REFERENCES

[1] Y.F. Ye, Q. Wang, J. Lu, C.T. Liu, Y. Yang, High-entropy alloy: challenges and prospects, Materials Today, Volume 19, Issue 6, 2016, Pages 349-362, ISSN 1369-7021, https://doi.org/10.1016/j.mattod.2015.11.026. (https://www.sciencedirect.com/science/article/pii/S1369702115004010)

[2] Tushar Sonar, Mikhail Ivanov, Evgeny Trofimov, Aleksandr Tingaev, Ilsiya Suleymanova, An overview of microstructure, mechanical properties and processing of high entropy alloys and its future perspectives in aeroengine applications, Materials Science for Energy Technologies, Volume 7, 2024, Pages 35-60, ISSN 2589-2991, https://doi.org/10.1016/j.mset.2023.07.004. (https://www.sciencedirect.com/science/article/pii/S258929912300040X)
See also: Li, Weidong & Wang, Gang & Wu, Shiwei & Liaw, Peter. (2018). Creep, fatigue, and fracture behavior of high-entropy alloys. Journal of Materials Research. 33. 1-24. 10.1557/jmr.2018.191.

[3] Yuan Wu, Fei Zhang, Xiaoyuan Yuan, Hailong Huang, Xiaocan Wen, Yihan Wang, Mengyuan Zhang, Honghui Wu, Xiongjun Liu, Hui Wang, Suihe Jiang, Zhaoping Lu, Short-range ordering and its effects on mechanical properties of high-entropy alloys, Journal of Materials Science & Technology, Volume 62, 2021, Pages 214-220, ISSN 1005-0302, https://doi.org/10.1016/j.jmst.2020.06.018. (https://www.sciencedirect.com/science/article/pii/S1005030220306083)

[4] Cláudio Geraldo Schön, On short-range order strengthening and its role in high-entropy alloys, Scripta Materialia, Volume 196, 2021, 113754, ISSN 1359-6462, https://doi.org/10.1016/j.scriptamat.2021.113754. (https://www.sciencedirect.com/science/article/pii/S1359646221000348)

[5] L.R. Owen, H.Y. Playford, H.J. Stone, M.G. Tucker, Analysis of short-range order in Cu3Au using X-ray pair distribution functions, Acta Materialia, Volume 125, 2017, Pages 15-26, ISSN 1359-6454, https://doi.org/10.1016/j.actamat.2016.11.048. (https://www.sciencedirect.com/science/article/pii/S1359645416309156)

APPENDIX

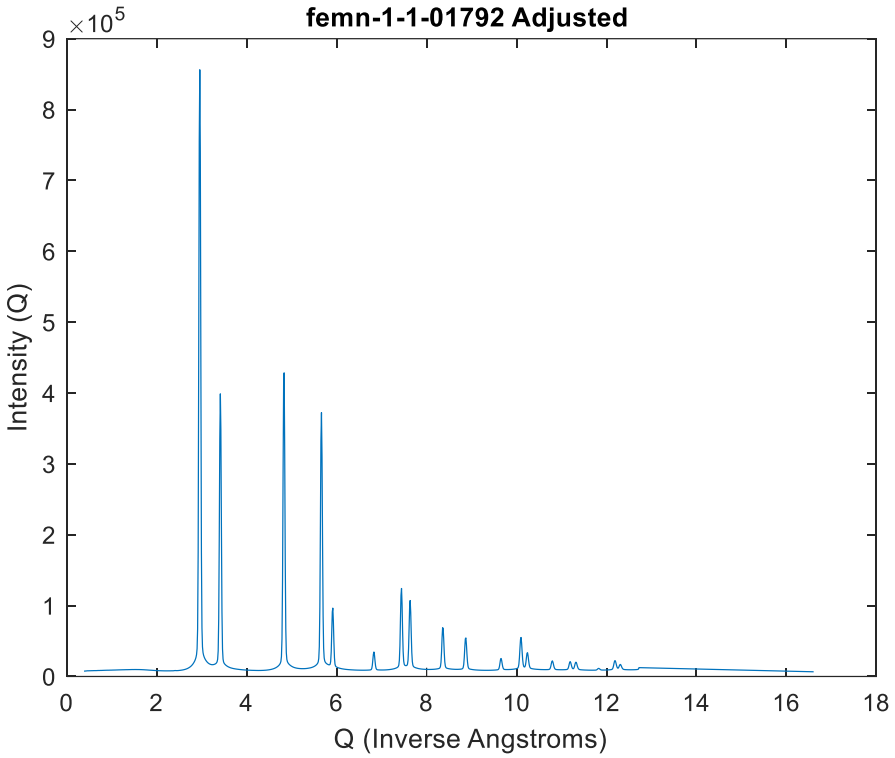

Figure 4. Plot of experimental data for femn-1-1-01792 after adjustment

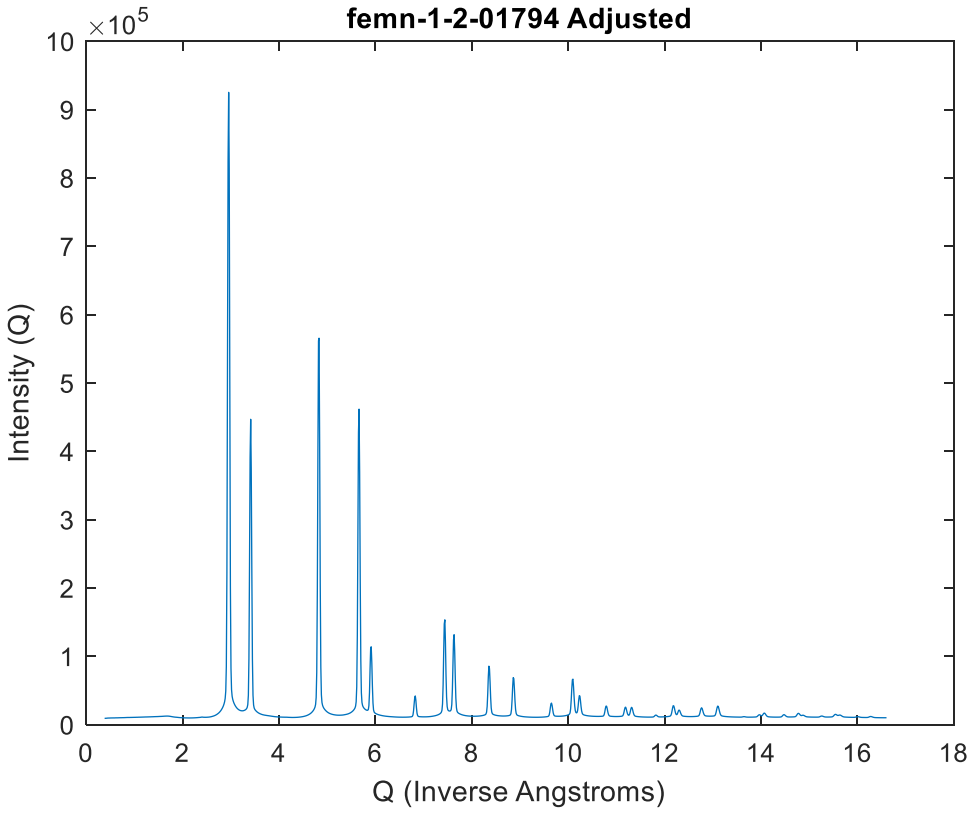

Figure 5. Plot of experimental data for femn-1-2-01794 after adjustment

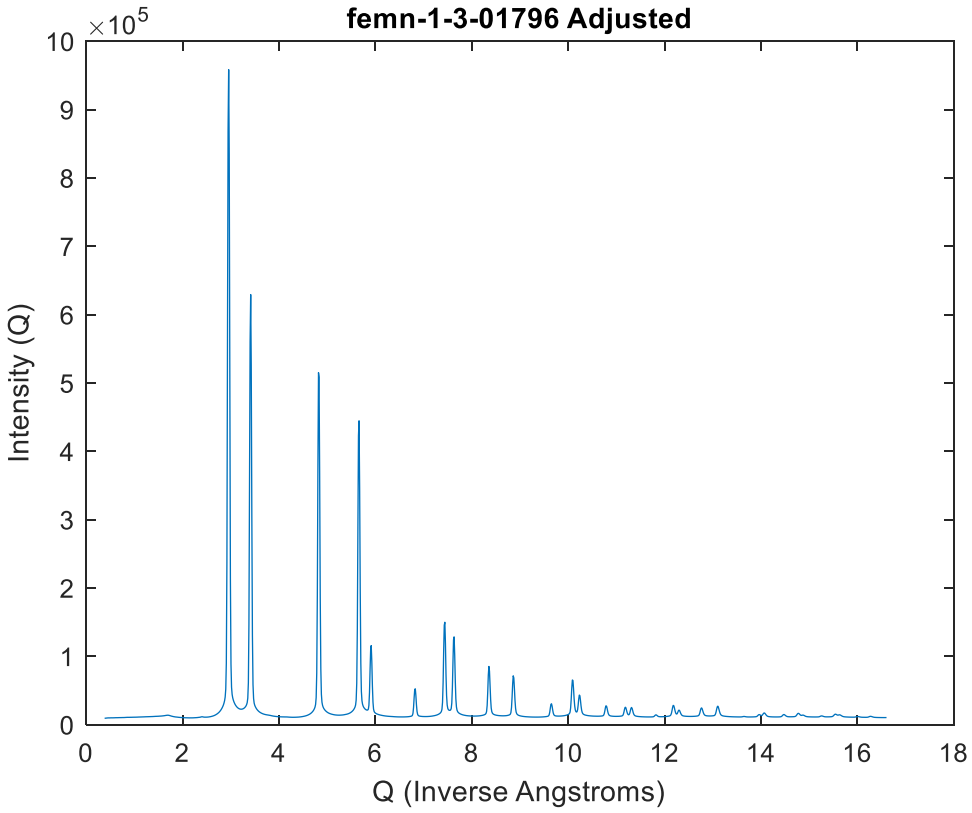

Figure 6. Plot of experimental data for femn-1-3-01796 after adjustment

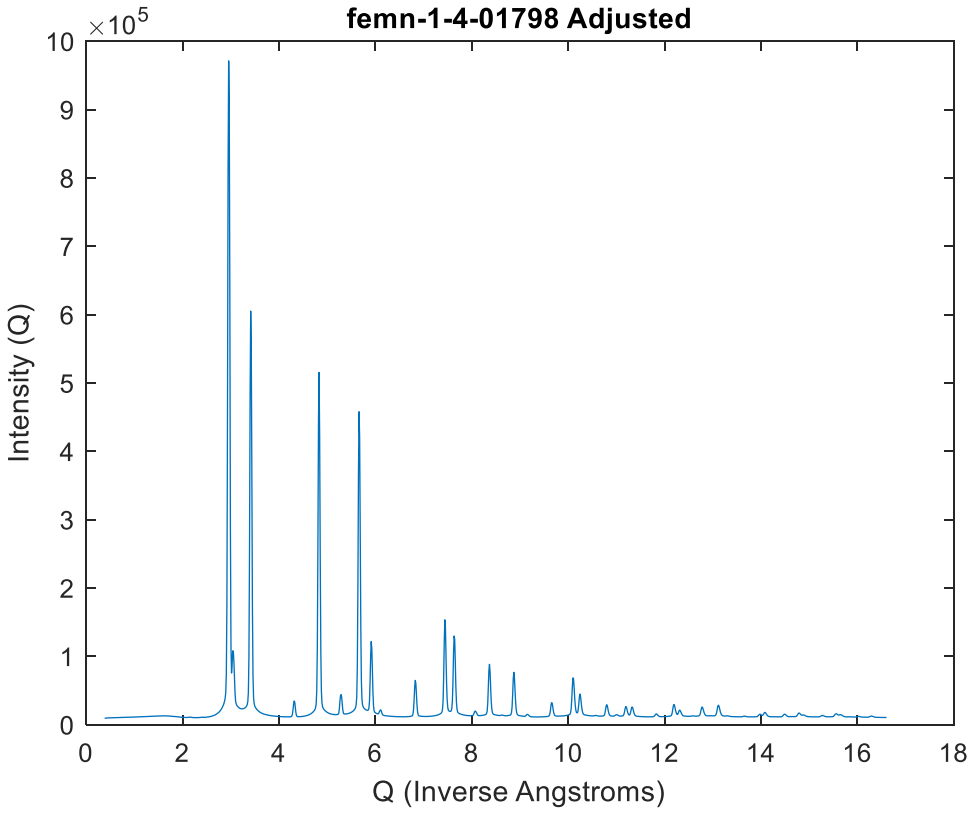

Figure 7. Plot of experimental data for femn-1-4-01798 after adjustment

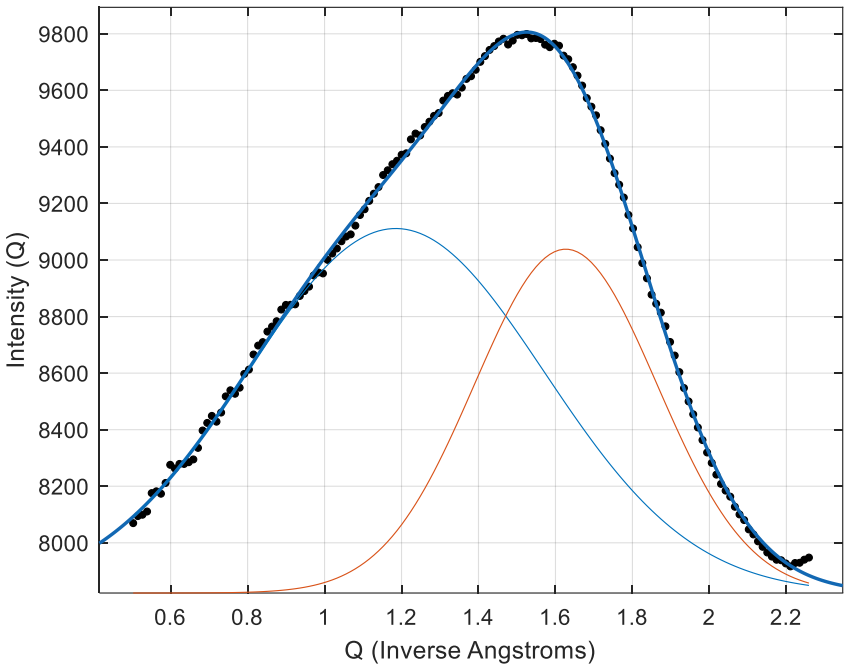

Figure 8. Curve fitting overlay using gaussian peaks for the femn-1-1-01792 sample

Goodness of Fit:

SSE = 5.4124e+04
R-Square = 0.9990
DFE = 140
Adj R-Square = 0.9990
RMSE = 19.6621

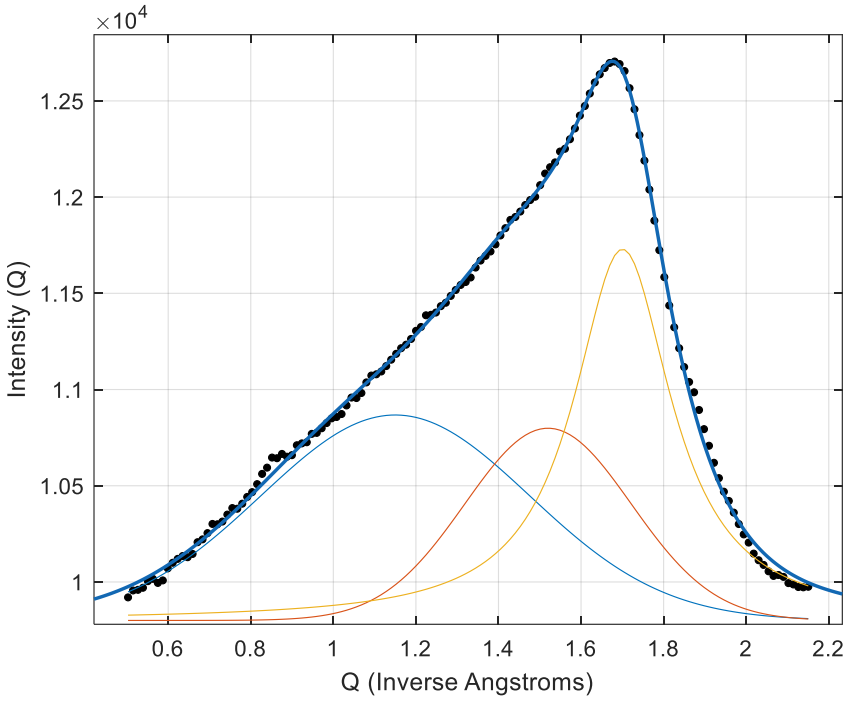

Figure 9. Curve fitting overlay using gaussian and Lorentzian peaks for the femn-1-2-01794 sample

Goodness of Fit:

SSE = 1.3703e+05
R-Square = 0.9985
DFE = 131
Adj R-Square = 0.9985
RMSE = 32.3427

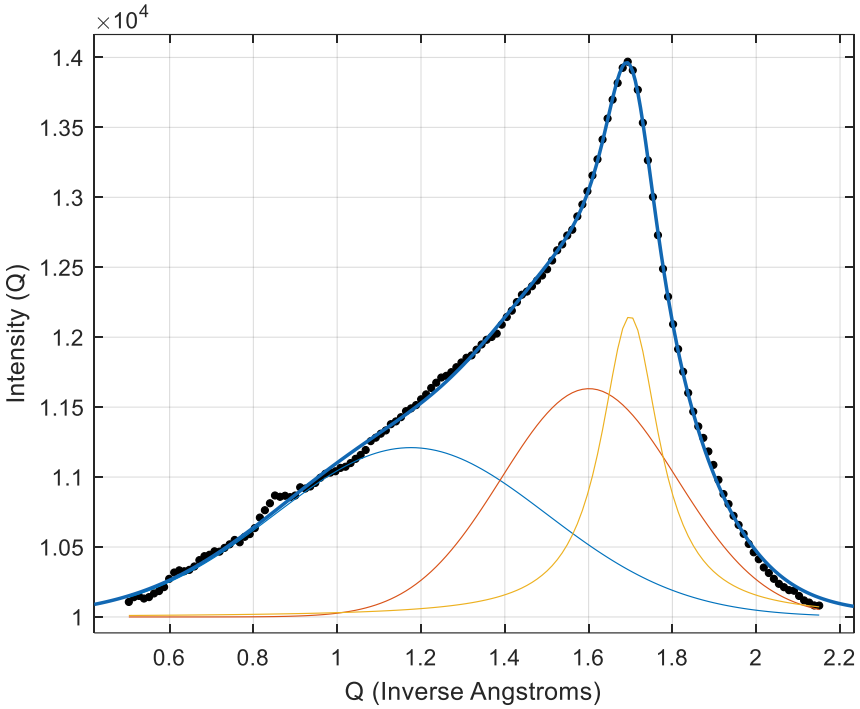

Figure 10. Curve fitting overlay using gaussian and Lorentzian peaks for the femn-1-3-01796 sample

Goodness of Fit:

SSE = 1.7762e+05
R-Square = 0.9988
DFE = 128
Adj R-Square = 0.9987
RMSE = 37.2517

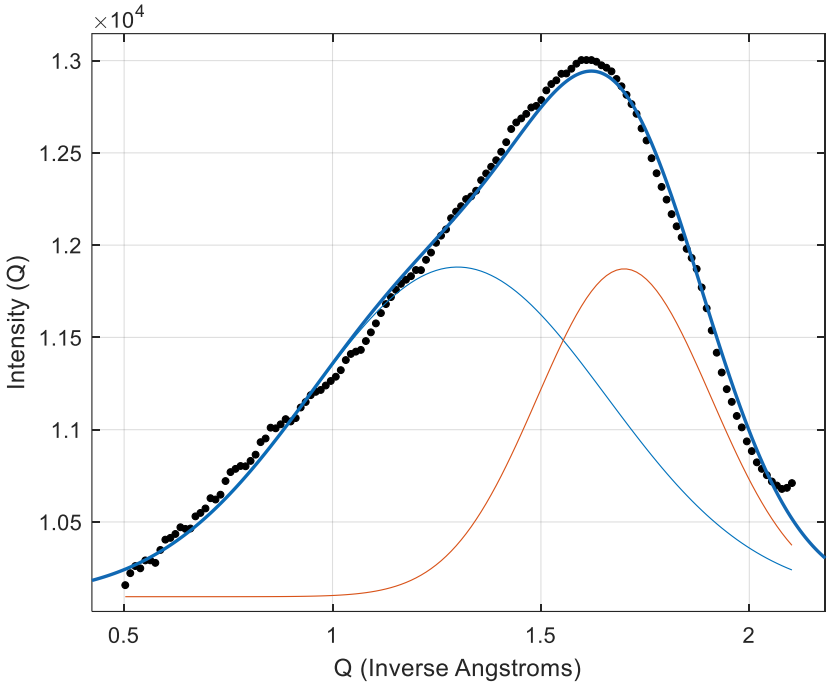

Figure 11. Curve fitting overlay using gaussian peaks for the femn-1-4-01798 sample

Goodness of Fit:

SSE = 6.3173e+05
R-Square = 0.9937
DFE = 129
Adj R-Square = 0.9935
RMSE = 69.9796

Short-Range Order Parameters

femn-1-1-01792 sample
(D1) Area under curve = 1.6498e+04

femn-1-2-01794 sample
(D2) Area under curve = 1.9773e+04

femn-1-3-01796 sample
(D3) Area under curve = 2.0363e+04

femn-1-4-01798 sample
(D4) Area under curve = 1.9805e+04

Normalization of Short-Range Order Parameters

$D1/I_{111}(1) = (1.6498e+04)/(5.6159e+04) = 0.2938$

$D2/I_{111}(2) = (1.9773e+04)/(6.1101e+04) = 0.3236$

$D3/I_{111}(3) = (2.0363e+04)/(6.5153e+04) = 0.3125$

$D4/I_{111}(4) = (1.9805e+04)/(6.1420e+04) = 0.3225$

Full Width at Half-Maximum (Overall Peak)

femn-1-1-01792 sample
FWHM = 1.1956

femn-1-2-01794 sample
FWHM = 1.1207

femn-1-3-01796 sample
FWHM = 1.1540

femn-1-4-01798 sample
FWHM = 1.1207

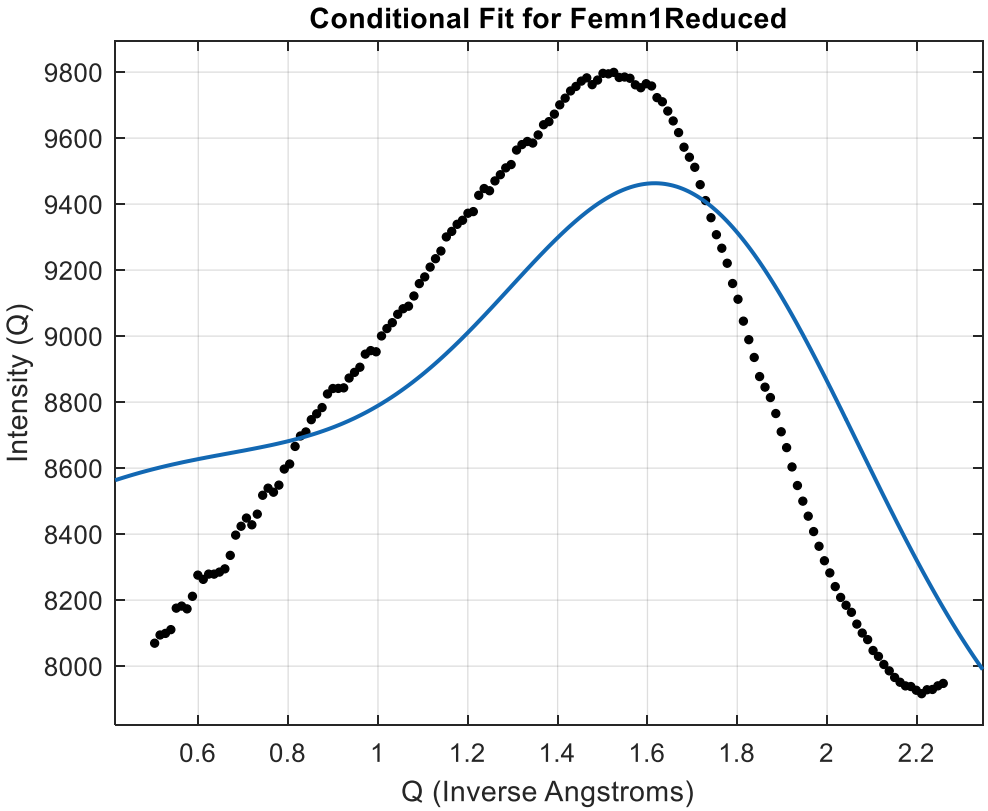

Figure 12. First conditional fitting attempt for femn-1-1-01792 using Q values from initial indexes

Sample 1 Gaussian Peak 1: Q = 0.603 Inverse Angstroms
Sample 1 Gaussian Peak 2: Q = 1.703 Inverse Angstroms

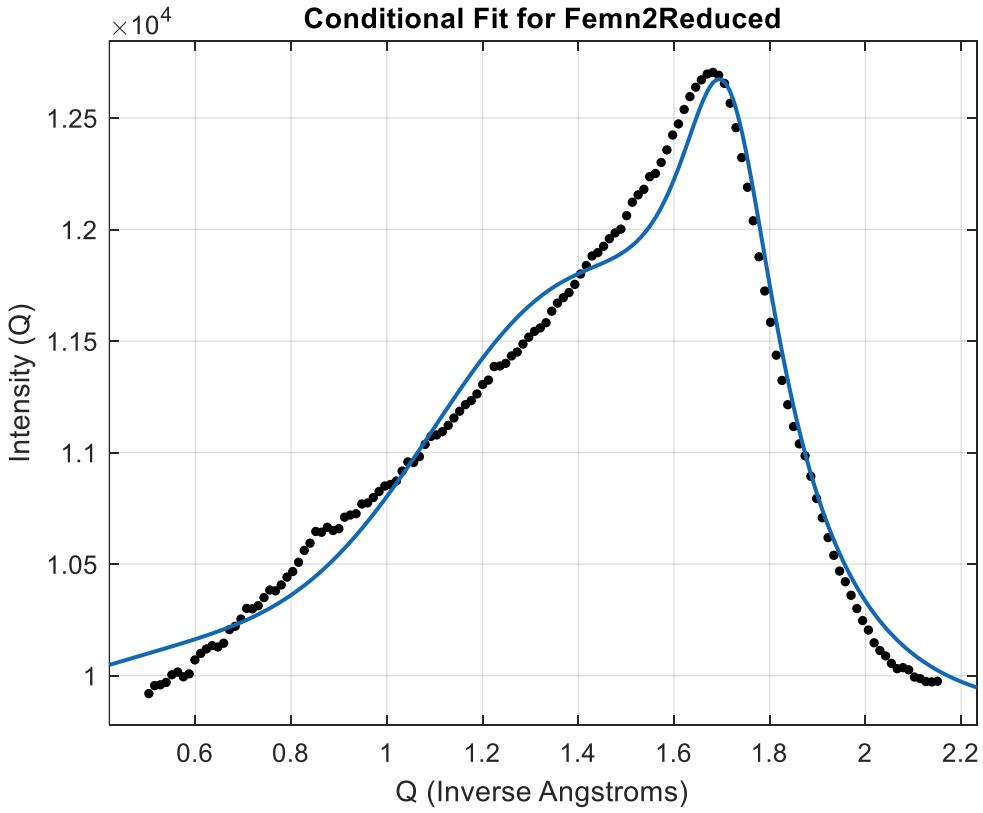

Figure 13. First conditional fitting attempt for femn-1-2-01794 using Q values from initial indexes

Sample 2 Gaussian Peak 1: Q = 0.609 Inverse Angstroms
Sample 2 Gaussian Peak 2: Q = 1.361 Inverse Angstroms
Sample 2 Lorentzian Peak 1: Q = 1.721 Inverse Angstroms

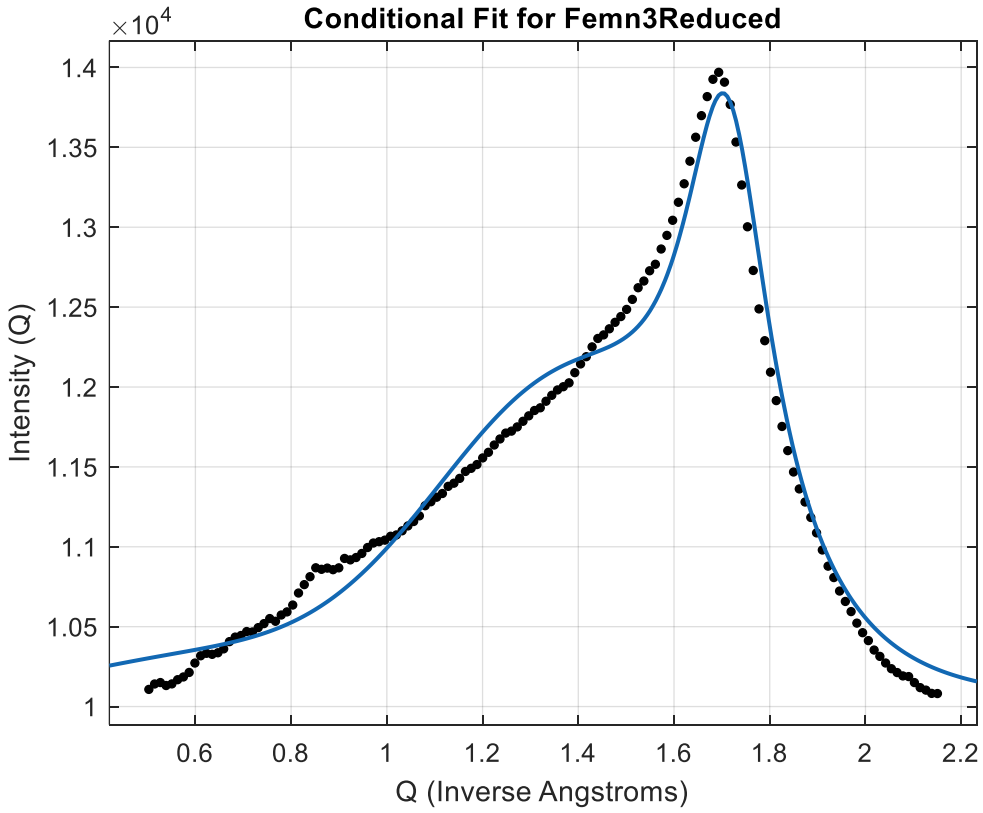

Figure 14. First conditional fitting attempt for femn-1-3-01796 using Q values from initial indexes

Sample 3 Gaussian Peak 1: Q = 0.609 Inverse Angstroms
Sample 3 Gaussian Peak 2: Q = 1.361 Inverse Angstroms
Sample 3 Lorentzian Peak 1: Q = 1.721 Inverse Angstroms

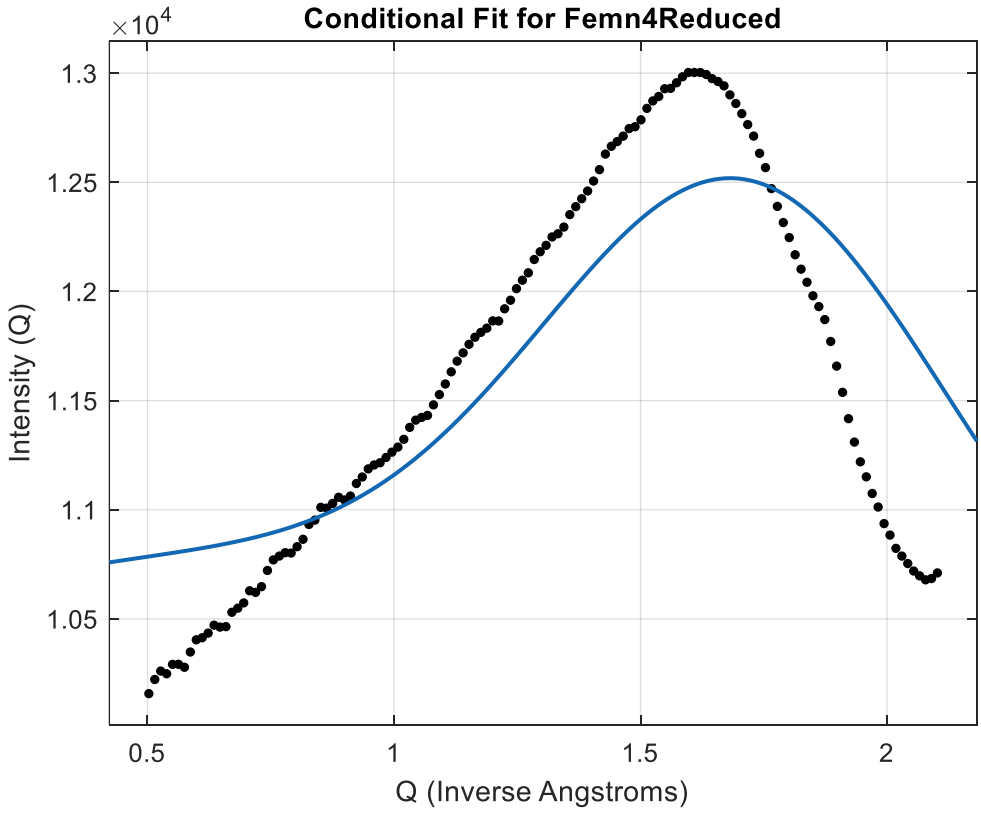

Figure 15. First conditional fitting attempt for femn-1-4-01798 using Q values from initial indexes

Sample 4 Gaussian Peak 1: Q = 0.613 Inverse Angstroms
Sample 4 Gaussian Peak 2: Q = 1.732 Inverse Angstroms

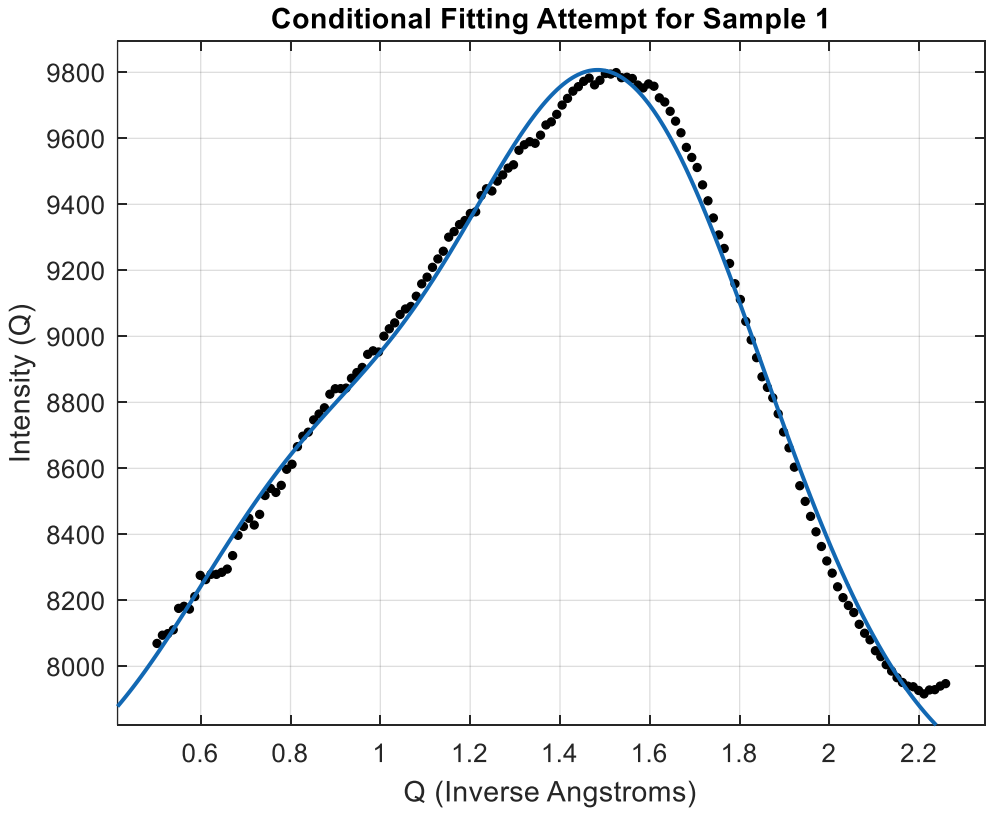

Figure 16. Example of improvement in conditional fitting of Sample 1 after adjusting Q values

Percent Error of Q Values = (Conditional Fit - Original) / Original

Example of Q Value Comparison (Percent Error) for the first gaussian peak of Sample 1 = ((0.8010 – 1.1850) / 1.1850) x 100 = -32.40%

Example of Q Value Comparison (Percent Error) for the second gaussian peak of Sample 1 = ((1.5 – 1.6267) / 1.6267) x 100 = -7.78%

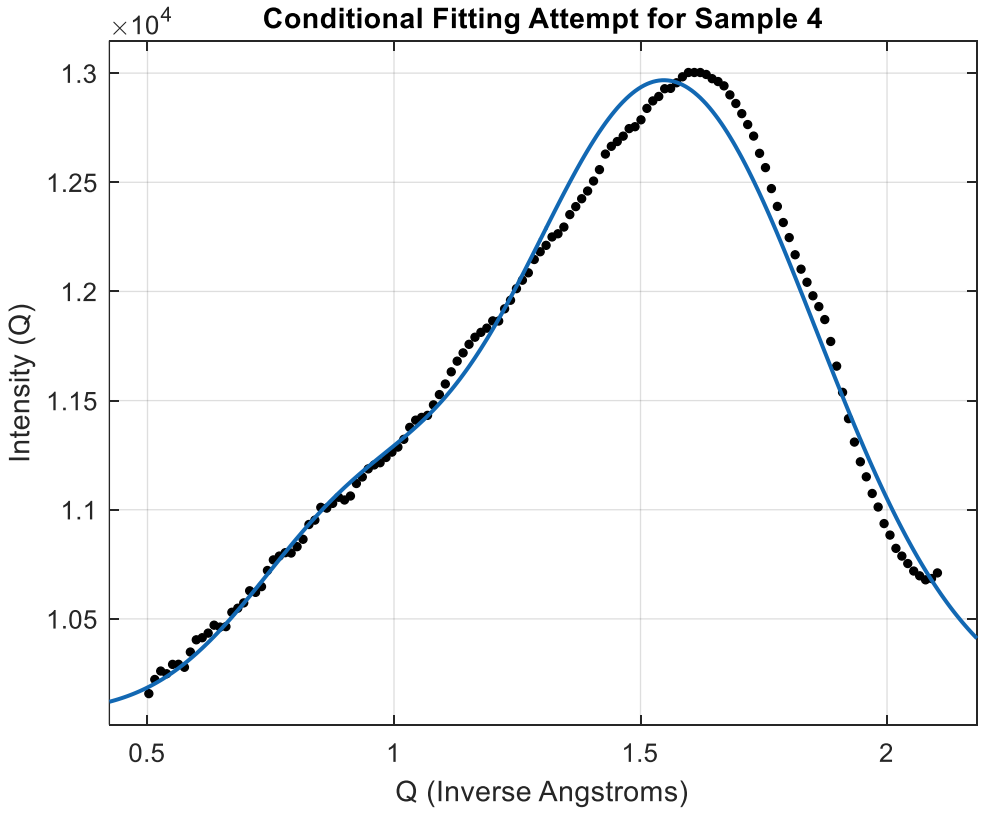

Figure 17. Example of improvement in conditional fitting of Sample 4 after adjusting Q values

Example of Q Value Comparison (Percent Error) for the first gaussian peak of Sample 4 = ((0.9 – 1.3) / 1.3) x 100 = -30.77%

Example of Q Value Comparison (Percent Error) for the second gaussian peak of Sample 4 = ((1.55 – 1.7) / 1.7) x 100 = -8.82%

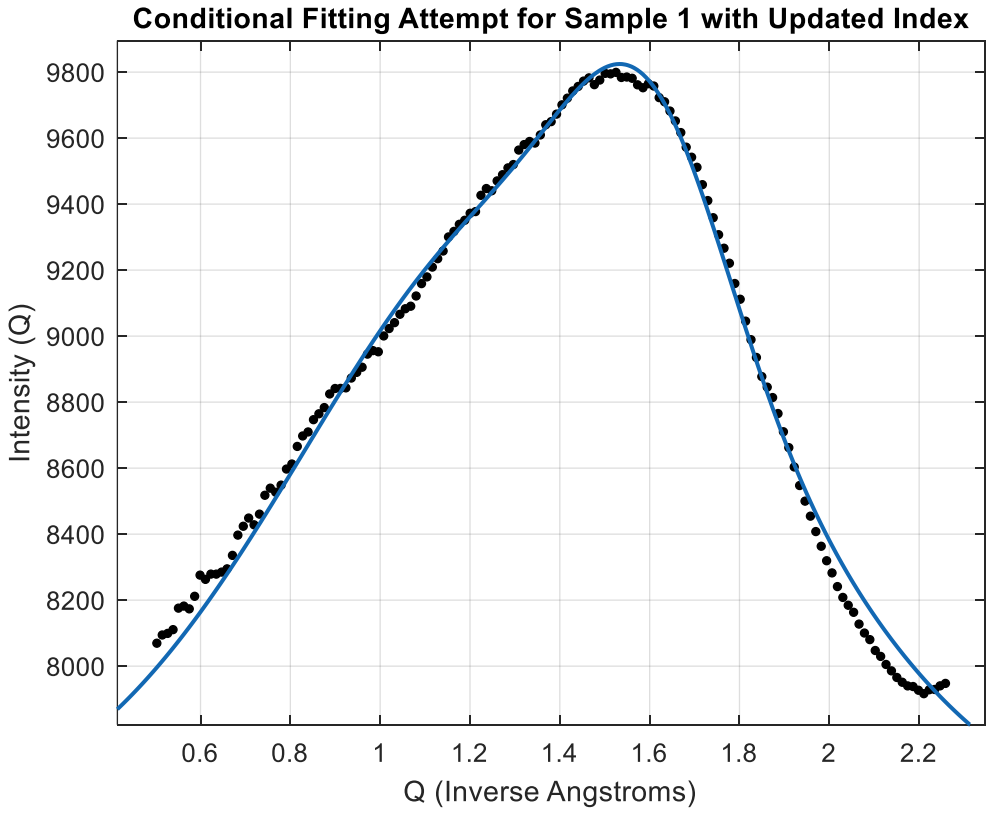

Figure 18. Example of improvement in conditional fitting using an updated index for the first gaussian peak in Sample 1

Example of Q Value Comparison (Percent Error) for the first gaussian peak of Sample 1 = ((1.345 – 1.1850) / 1.1850) x 100 = 13.5%

Example of Q Value Comparison (Percent Error) for the second gaussian peak of Sample 1 = ((1.6 – 1.6267) / 1.6267) x 100 = -1.64%

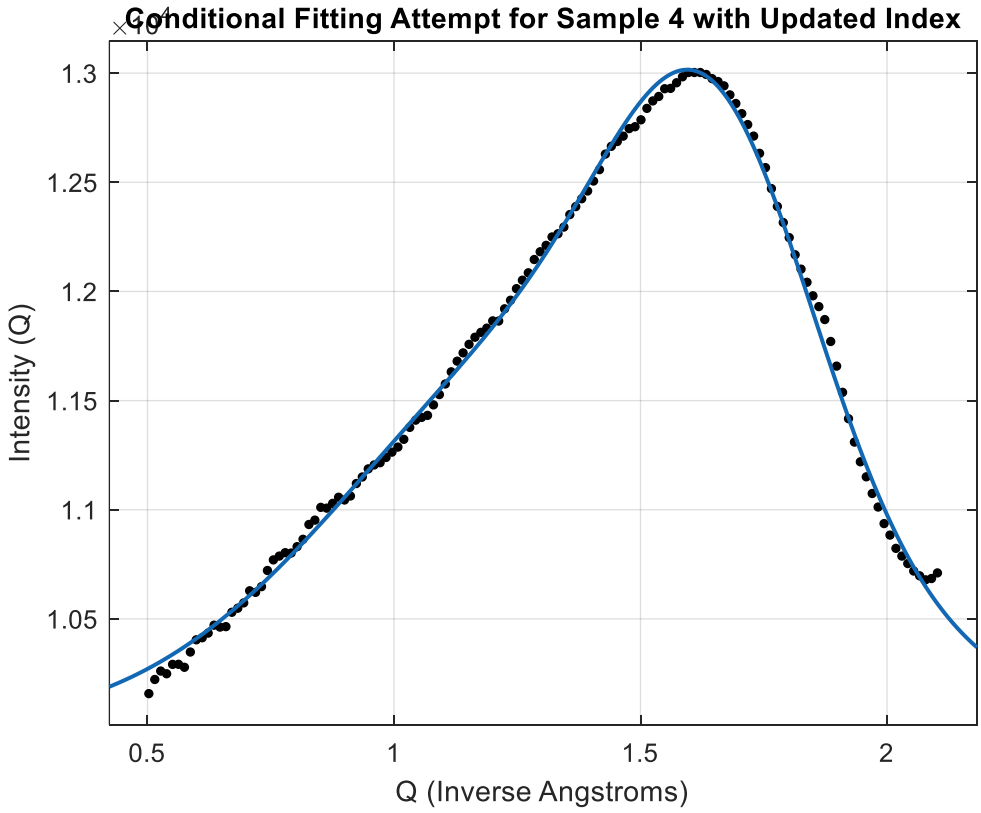

Figure 19. Example of improvement in conditional fitting using an updated index for the first gaussian peak in Sample 4

Example of Q Value Comparison (Percent Error) for the first gaussian peak of Sample 4 = ((1.3606 – 1.3) / 1.3) x 100 = 4.66%

Example of Q Value Comparison (Percent Error) for the second gaussian peak of Sample 4 = ((1.65 – 1.7) / 1.7) x 100 = -2.94%

Table 1. Comparison of Previous Indexes to Improved Indexes

Sample 1 First Gaussian Peak	(0.5, 0.5, 0)	(0.25, 0.75, 0)
Sample 1 Second Gaussian Peak	(1, 0, 0)	(1, 0, 0)
Sample 4 First Gaussian Peak	(0.5, 0.5, 0)	(0.25, 0.75, 0)
Sample 4 Second Gaussian Peak	(1, 0, 0)	(1, 0, 0)

Table 2. Calculated Lattice Parameters for the Four Samples

femn-1-1-01792 (Sample 1)	3.689 Angstroms
femn-1-2-01794 (Sample 2)	3.651 Angstroms
femn-1-3-01796 (Sample 3)	3.651 Angstroms
femn-1-4-01798 (Sample 4)	3.627 Angstroms

Table 3. Peak Width and Peak Height for Gaussian Peaks of First and Fourth Samples

Gaussian Peaks	FWHM	Number of Unit Cells	Peak Height (Q Space)	Peak Height x Sigma Q	Strength Rank
Sample 1 First Gaussian Peak	3.136 Angstroms	0.850	1.8977e+03	1379.82	1
Sample 1 Second Gaussian Peak	9.4488 Angstroms	2.561	593.6066	143.237	8
Sample 4 First Gaussian Peak	3.658 Angstroms	1.009	1.8238e+03	1136.592	2
Sample 4 Second Gaussian Peak	7.9057 Angstroms	2.180	1.4857e+03	428.476	5

Table 4. Peak Width and Peak Height for Gaussian and Lorentzian Peaks of Second and Third Samples

Peaks	FWHM	Number of Unit Cells	Peak Height (Q Space)	Peak Height x Sigma Q	Strength Rank
Sample 2 First Gaussian Peak	5.7 Angstroms	1.561	276.1917	110.477	10
Sample 2 Second Gaussian Peak	5.543 Angstroms	1.518	1.6327e+03	671.530	4
Sample 2 First Lorentzian Peak	8.105 Angstroms	2.220	920.1804	258.847	6
Sample 3 First Gaussian Peak	5.407 Angstroms	1.4810	267.4206	112.77	9
Sample 3 Second Gaussian Peak	5.610 Angstroms	1.537	1.8300e+03	743.712	3
Sample 3 First Lorentzian Peak	10.1118 Angstroms	2.770	1.0299e+03	232.242	7

VITA

Mariah Wakefield is from Arlington, Tennessee. She graduated from Vanderbilt University with a Bachelor of Engineering in December 2018, having studied Chemical Engineering. She is currently pursuing a Master of Science at the University of Tennessee-Knoxville while working as a Graduate Research Assistant in Materials Science and Engineering with Takeshi Egami, PhD at Oak Ridge National Laboratory in Oak Ridge, Tennessee.